IEEE Photonics Journal
An IEEE Photonics Society Publication

Open Access

Multiple Optical Compensation in Interferometric Fiber-Optic Gyroscope for Polarization Nonreciprocal Error Suppression

Volume 6, Number 5, October 2014

Ping Lu
Zinan Wang
Yi Yang
Dayu Zhao
Siyadong Xiong
Yulin Li
Chao Peng
Zhengbin Li

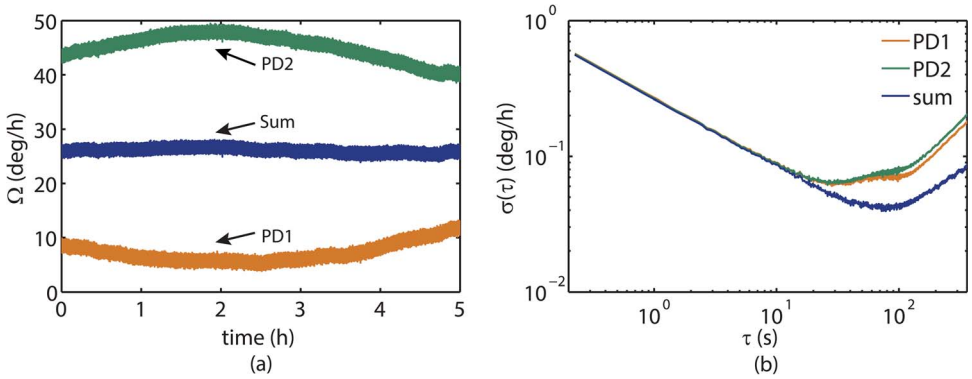

DOI: 10.1109/JPHOT.2014.2345887
1943-0655 © 2014 IEEE

IEEE photonics SOCIETY

IEEE

Multiple Optical Compensation in Interferometric Fiber-Optic Gyroscope for Polarization Nonreciprocal Error Suppression

Ping Lu, Zinan Wang, Yi Yang, Dayu Zhao, Siyadong Xiong, Yulin Li, Chao Peng, and Zhengbin Li

State Key Laboratory of Advanced Optical Communication Systems and Networks, Department of Electronics, Peking University, Beijing 100871, China

DOI: 10.1109/JPHOT.2014.2345887

Manuscript received May 8, 2014; revised July 26, 2014; accepted July 30, 2014. Date of publication August 8, 2014; date of current version September 18, 2014. This work was supported by the 973 Program of China under Grant 2013CB329205 and by the National Natural Science Foundation of China under Grant 61307089. Corresponding author: C. Peng (e-mail: pengchao@pku.edu.cn).

Abstract: Polarization nonreciprocal (PN) errors within a novel interferometric fiber-optic gyroscope (IFOG) configuration are investigated both theoretically and experimentally. Different from those conventional IFOGs, here, two orthogonal polarizations coexist, and light can travel through multiple paths. The PN errors of individual paths possess opposite signs and, thus, can be effectively canceled out through a multiple optical compensation process. As experimentally demonstrated, the long-term stability of IFOG has been remarkably improved. From the perspective of optical compensation, the concept of "reciprocity" can be understood in a more generalized way.

Index Terms: Fiber-optic gyrocope, optical compensation.

1. Introduction

The interferometric fiber-optic gyroscope (IFOG), which is an inertial sensor that detects Sagnac phase shift between two counter-propagating waves, has been intensively investigated over decades for civilian and military applications [1], [2]. Since firstly been experimentally observed in 1976 [3], the polarization nonreciprocity (PN) has been recognized as one of the major causes of nonreciprocal phase errors in IFOGs that significantly degrades its performance of stability. Conventionally, the PN error is suppressed by maintaining a single polarization. This approach has been verified in both polarization maintaining IFOGs (PM-IFOGs) [6], [7] and depolarized IFOGs [8]–[10]. The well-known "minimal scheme" [4] is a typical and widely applied structure to eliminate PN errors, in which a polarizer with high polarization-extinction ratio (PER) is indispensable and light returning to photodiodes travels through polarization reciprocal paths.

Recently, a new alternative approach of PN error suppression was proposed [11]–[14]. It is proved that when two orthogonal and incoherent polarizations simultaneously propagate in IFOGs, they experience the same PN error but have opposite polarities. As a result, the overall PN error can be suppressed by summing up the intensity of two polarizations, and this process was referred to as "optical compensation". The optical compensation approach was first proposed in a dual-polarization IFOG [11] with a PM-fiber coil. After that, it has been extended to

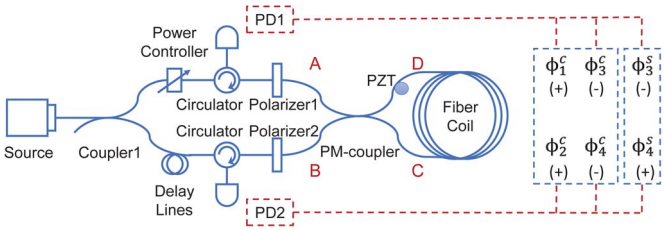

Fig. 1. Configuration of the IFOG based on multiple optical compensation, containing an amplified spontaneous emission (ASE) source (central wavelength 1550 nm; bandwidth 70 nm), a single-mode coupler (Coupler 1, 50 : 50), two circulators, two photo-detectors (PDs), two polarizers (PER 30 dB), a biaxial polarization maintaining coupler (PM-coupler), and a 2 km single mode fiber (SMF) coil.

TABLE 1

List of light paths

	reciprocal paths		nonreciprocal paths	
	path 1	path 2	path 3	path 4
CW beams	$A \to D \to C \to A$	$B \to D \to C \to B$	$B \to D \to C \to A$	$A \to D \to C \to B$
CCW beams	$A \to C \to D \to A$	$B \to C \to D \to B$	$B \to C \to D \to A$	$A \to C \to D \to B$

single-mode (SM) fiber coil and the structure complexity has been greatly simplified by employing Lyot depolarizers [12]–[14]. A comprehensive analysis indicates that, the optical compensation can reach the same theoretical limit on PN error suppression when comparing with polarization maintaining approach. In this case, the non-reciprocal port of IFOG becomes reciprocal, and the "minimal scheme" is no longer necessary. As a result, ultra-simple IFOG configuration with only one coupler can be realized [14].

The concept of optical compensation gives hints to other possible configurations for PN error suppression, in which the "reciprocity" can be understood in a more generalized way. In this work, we propose and demonstrate a novel structure that consists of multiple light paths and output ports. Although each output port is recognized as non-reciprocal in conventional concept, the overall PN error can still been eliminated by combining the signals from multiple ports. We refer to this phenomenon as "multiple optical compensation."

The remainder of this paper is organized as follows: In Section 2, we describe the optical configuration of an IFOG with multiple optical compensation, and present a theoretical model for PN error analysis; In Section 3, we present some simulation and experimental results, as well as some discussions. Finally, we state a summary of our work in Section 4.

2. Configuration and Theory

The configuration of IFOG based on multiple optical compensation is shown in Fig. 1. Since optical compensation requires two orthogonal polarizations simultaneously, the light from ASE source is split into two beams at Coupler 1 and then polarized along two orthogonal axes separately. Meanwhile, an optical delay line is placed on one arm to ensure the two polarizations are incoherent. On the other arm, a power controller is adopted to balance their power. It can be readily noticed that, after two orthogonal polarizations traveling through the biaxial PM-coupler and getting into the SMF coil, they experience multiple light paths and sum up at PD1 and PD2 respectively. We analyze the characteristics of the structure and PN errors of individual light paths as follows.

2.1. Structure Principle

We assume that the light is polarized at Polarizer 1 along X direction, and at Polarizer 2 along Y direction respectively, where X and Y directions are orthogonal. We denote 4 ports of the PM-coupler as points A,B,C and D, which are shown in Fig. 1. All possible light paths are listed in Table 1. Polarization X traveling clockwise (CW) is taken for an example. Since the beam

starting at Point A will end at either Point A or Point B, it forms two possible light paths (i.e., Path 1 and 4). Similarly, polarization Y also involves two possible light paths in CW direction (i.e., Path 2 and 3). According to the conventional definition of "reciprocity", Path 1 and 2 are reciprocal because the beams travel through the coupler and fiber coil, then back to their original start points. In contrast, Path 3 and 4 are nonreciprocal because the beams start from one point (A point for instance) but end at the opposite point (B point accordingly).

It is well known that the "reciprocity" is the fundamental requirement of IFOGs. Conventionally, it requests that light travels along exactly the same path for a given polarization, and hence, the port of coupler that light enters the fiber coil should be exactly the same port that light leaves. In conventional PM and depolarized IFOGs, unacceptable PN error will be brought in if the reciprocity is broken. According to this rule, it seems that the proposed configuration can not work because several nonreciprocal paths participate. However, as we prove in the following section, although PN errors exists among individual light paths, they are in opposite signs and can be potentially canceled out in the meaning of "multiple optical compensation."

2.2. Analysis of PN Errors

We use Jones matrix method to model the PN errors in each light paths of the proposed configuration [4], [15], and the detailed derivations are presented in Appendix section. The PN errors were caused by the inter-couplings between two individual polarizations. In the proposed configuration, the polarizers of limited PER and the SMF coil contribute polarization couplings simultaneously. As shown in the inset of Fig. 1, we classify the PN errors into two categories ϕ_n^s and ϕ_n^c, where n denotes the path number. ϕ_n^s represents the PN error that purely contributed by the polarization couplings inside fiber coils. Since we adopt an SMF coil, these terms should be considerably large and may statistically evolves with time. On the other hand, ϕ_n^c depicts the PN error associated with at least one polarizer. Because the polarizers have high PER, these terms are relatively smaller and more stable.

The theoretical model indicates several characteristics of the PN errors. Firstly, the dominant PN error ϕ_n^s only exists in nonreciprocal paths, i.e., Path 3 and 4; but these errors have opposite signs in two individual paths as shown by Eq. (9), owing to the symmetry of polarizations. It means these errors can be effectively eliminated by summing up the optical intensity. Besides, the relatively small PN errors ϕ_n^c appear in both reciprocal and nonreciprocal paths, and they also have determined relationship in polarities. As shown in Eq. (10), the PN errors in reciprocal paths ϕ_1^c and ϕ_2^c have opposite signs to the PN errors of nonreciprocal paths ϕ_3^c and ϕ_4^c. Hence, ϕ_n^c can also be canceled out by the optical compensation. From the perspective described above, optical compensation does not only occur between nonreciprocal paths, but also happen among reciprocal paths and nonreciprocal paths. It implies multiple compensation is realized, which further increases the efficiency of optical compensation.

Practically, the angular velocity detected at each PD is a comprehensive result related to both a reciprocal and a nonreciprocal path. PN errors of two PDs have opposite signs, which are derived as

$$\phi_{err}^{pd1} = \arctan \frac{-w_2 \left|C_3^* C_2\right|^2 \sin\phi_{32} + (w_2\varepsilon_y - w_1\varepsilon_x)u_2}{w_1 \left|C_1\right|^2 - w_2 \left|C_3^* C_2\right|^2 \cos\phi_{32} + (w_1\varepsilon_x - w_2\varepsilon_y)u_1}$$
$$\phi_{err}^{pd2} = \arctan \frac{w_1 \left|C_3^* C_2\right|^2 \sin\phi_{32} - (w_2\varepsilon_y - w_1\varepsilon_x)u_2}{w_2 \left|C_4\right|^2 - w_1 \left|C_3^* C_2\right|^2 \cos\phi_{32} + (w_1\varepsilon_x - w_2\varepsilon_y)u_1}. \quad (1)$$

Therefore, when summing up angular velocities of two PDs, PN errors of the IFOG are suppressed efficiently by multiple optical compensation, which is shown as Eq. (2). It is noteworthy that, two polarizers with high PER to realize two stable orthogonal polarizations are

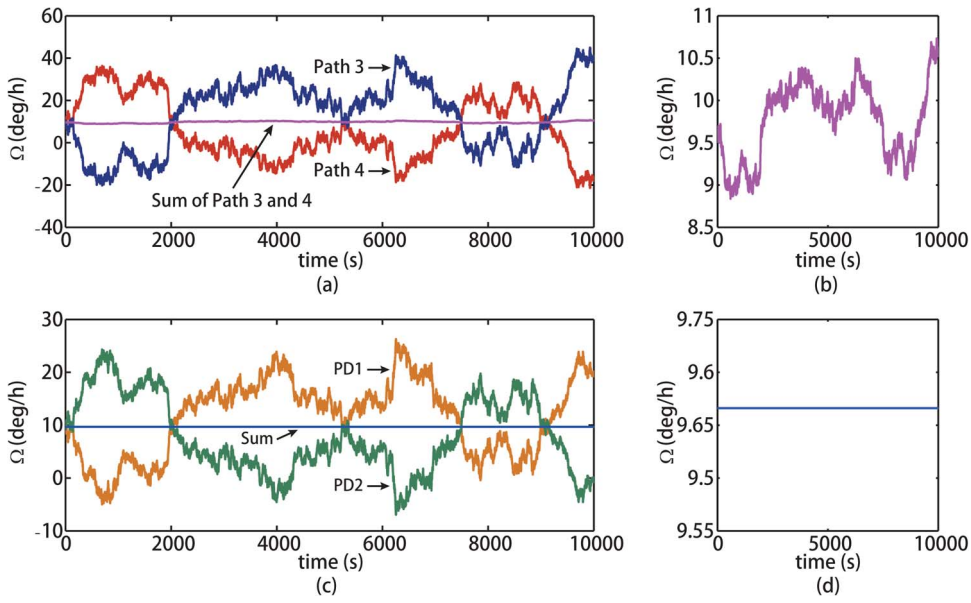

Fig. 2. Simulation of multiple optical compensation. (a) Angular velocities of nonreciprocal Path 3 (dark blue) and 4 (red) and sum of the two (purple). (b) Sum of the angular velocities of nonreciprocal paths. (c) Angular velocities detected at PD 1 (yellow) and PD2 (green) and overall noise (light blue). (d) Overall noise when power balance is achieved.

no longer indispensable, because errors ϕ_n^s are completely canceled out, even if polarizers posses low PER.

$$\phi_{err}^{sum} = \arctan \frac{(w_1 - w_2)\left|C_3^* C_2\right|^2 \sin \phi_{32}}{w_1 |C_1|^2 + w_2 |C_4|^2 - (w_1 + w_2)\left|C_3^* C_2\right|^2 \cos \phi_{32} + 2(w_1 \varepsilon_x - w_2 \varepsilon_y) u_1}. \tag{2}$$

As the formulae indicate, the power balance is critical for establishing effective compensation. Power balance, denoted as $\Delta w = w_1 - w_2$, represents the power difference between two polarizations. It depends on the splitting ratio of Coupler 1, insertion loss and other factors. When Δw equals zero, optical compensation will achieve complete PN error elimination as shown in Eq. (2). In our experiment, we introduce a power controller to carefully balance the power.

3. Results and Discussions

A numerical simulation was performed to analyze characteristics of the multiple optical compensation. Fig. 2(a) illustrates the demodulated angular velocities with nonreciprocal Path 3 and 4. Due to the PN errors that determined by Eq. (8), the angular velocities were randomly evolving with time in considerably large amplitudes, but their polarities were always opposite. In fact, the PN errors with Path 3 and 4 include both ϕ_n^s and ϕ_n^c components that follow Eqs. (9) and (10) respectively, in which the ϕ_n^s components are dominant. When summing up the results of Path 3 and 4, the ϕ_n^s components of PN errors cancel out with each other. As a result shown in Fig. 2(b), the angular velocity becomes relatively stable and only shows some small random variations determined by the remaining ϕ_n^c component.

In practice, the angular velocities of Path 3 and 4 are not able to measure independently since they are always mixed with the light from Path 1 and 2. The simulation results in Fig. 2(c) present the demodulated angular velocities from PD 1 and 2 that we can measure in experiments. As shown in Eq. (11), the PN errors detected at PD 1 and 2 contain the contribution

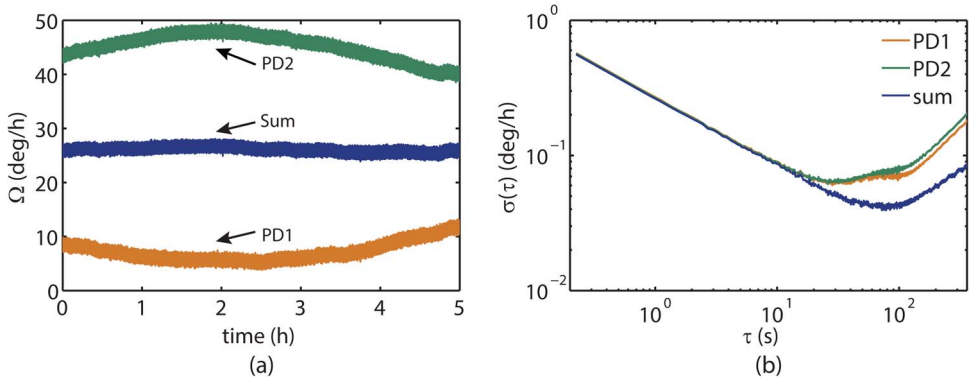

Fig. 3. Experimental observation of multiple optical compensation. (a) Time domain output. (b) Allan variance analysis: angular velocities detected by PD 1 (yellow), PD 2 (green), and sum of two (blue).

TABLE 2

Allan variance indices

	Rate ramp ($^\circ/h^2$)	Bias drift ($^\circ/h$)	Rate random walk ($^\circ/h^{3/2}$)	Angle random walk ($^\circ/h^{1/2}$)
PD1	1.2426	0.0688	0.5587	0.0050
PD2	1.7559	0.0602	0.2084	0.0054
Sum	0.2401	0.0373	0.3609	0.0055

from multiple light paths. More specifically, PD 1 combines contribution from Path 1 and 3 while PD 2 combines contribution from Path 2 and 4. Due to the large random variations of the PN error of Path 3 and 4, the angular velocities detected at PD 1 and 2 also randomly vary with time. However, as shown in Fig. 2(d), the overall PN errors become completely eliminated if we sum up the results of PD 1 and 2, when power balance is achieved. In these cases, both ϕ_n^s and ϕ_n^c components are suppressed simultaneously. The simulation results agree with our analytical model.

To demonstrate the multiple optical compensation phenomenon experimentally, we carried out a stability test of the proposed configuration (see Fig. 3). We used a 2 km SMF coil which was horizontally placed on an optic platform. The Earth's rotation velocity was measured ($9.666^\circ/h$ at our lab location: 39.99° N). The experiment was performed in uncontrolled environment, therefore, the temperature fluctuation also induced PN errors. The demodulated angular velocities from PD 1 and 2 are presented in Fig. 3(a). As expected, they show behaviors similar to the simulation results shown in Fig. 2(d). The angular velocities demodulated from PD 1 and 2 possess opposite signs while varying over time. When summing them up, the compensated angular velocity becomes remarkably more stable.

It is noticed that the compensated angular velocity was not in its theoretical value ($9.666^\circ/h$) but contained a constant bias about $20^\circ/h$. This stable bias is caused by the coupler nonreciprocity (CN) error of PM coupler. As been verified, the CN bias is much more stable than PN errors even in an uncontrolled environment [13]. Therefore, it is not the performance limitation in most cases. The stable bias can be omitted conveniently when the scale factor of the IFOG is calibrated [14].

For clear comparison of the output stability, we calculate the Allan variances for the uncompensated results from PD 1 and 2, and also the compensated result, as presented in Fig. 3(b). The Allan curve of the compensated result is much lower than the other two, especially in long term scales. We also obtained the detailed noise indices of the proposed IFOG configurations, as given in Table 2. The long term noises (bias drift and rate ramp) are significantly suppressed in our design. Especially, bias drift is reduced form $6.88 \times 10^{-2^\circ}/h$ and $8.01 \times 10^{-2^\circ}/h$ to

3.73×10^{-2}°/h. This comparison proves that the multiple optical compensation effectively suppresses the PN errors.

As the theoretical model points out, power balance is crucial for effective suppression of PN errors through optical compensation. As shown in Eq. (2), the PN errors could be completely eliminated when the perfect power balance that $w_1 = w_2$ is established, which is similar to make the degree of polarization (denoted as d) approach to zero in the all-depolarized configuration of IFOG [12]. In experiments, the power was balanced by carefully tuning the power controller.

4. Conclusion

In conclusion, we propose a novel configuration of IFOG that effectively suppresses the PN errors. Comparing with the conventional PM and depolarized IFOGs in which maintaining one polarization state is indispensable, here two orthogonal polarizations exist simultaneously and light beams can travel though multiple paths. These paths can be reciprocal or nonreciprocal in conventional definition. However, as we proved theoretically and experimentally, the PN errors within multiple paths have opposite polarities, and thus can be potentially canceled out. We refer to this phenomenon as "multiple optical compensation."

Form the perspective of multiple optical compensation, the "reciprocity" can be understood in a more generalized way. The PN error can be either eliminated by keeping a single polarization in reciprocal paths, or alternatively, it can be optically compensated by summing up the optical intensity of multiple paths. As experimentally demonstrated, the proposed configuration has promising performance, particularly on long term stability.

APPENDIX
Matrix Analysis

We use Jones matrix method to analyze the PN error in the multiple optical compensation IFOG. Normalized light fields entering the IFOG are given as

$$\mathbf{E}_0 = \begin{bmatrix} E_{0x}(t) \\ E_{0y}(t) \end{bmatrix} e^{j\omega_0 t}. \tag{3}$$

The light is supposed to be polarized along X direction at Polarizer 1, and along Y direction at Polarizer 2, where X and Y directions are orthogonal. The matrices for the two polarizers are expressed as Eq. (4), where ε_1 and ε_2 are extinction coefficients.

$$\mathbf{P}_x = \begin{bmatrix} 1 & 0 \\ 0 & \varepsilon_1 \end{bmatrix}, \quad \mathbf{P}_y = \begin{bmatrix} \varepsilon_2 & 0 \\ 0 & 1 \end{bmatrix}. \tag{4}$$

As the light beams travel through nonreciprocal port of the PM-coupler, a phase shift of π is taken into account by a separated matrix as

$$k_{tm} = \sqrt{1 - k_m}, \quad k_{cm} = \sqrt{k_m} e^{j\frac{\pi}{2}}. \tag{5}$$

If light leaves the coupler at a direct port, the matrix is noted as k_{tm}; otherwise, the matrix is noted as k_{cm}. Here, m is the number of couplers, and k_m is the splitting ratio.

We utilize complex coefficient $\mathbf{w}_n$ to describe loss caused by fusing points and couplers, and loss influence is displayed in the following table. Here n is the path number, and the superscripts "+" and "−" stand for clockwise and counterclockwise, respectively.

n	1	2	3	4
$\mathbf{w}_n^+$	$k_{t1}k_{t2}k_{c2}$	$k_{c1}k_{c2}k_{t2}$	$k_{c1}k_{c2}k_{c2}$	$k_{c1}k_{c2}k_{c2}$
$\mathbf{w}_n^-$	$k_{t1}k_{c2}k_{t2}$	$k_{c1}k_{t2}k_{c2}$	$k_{c1}k_{t2}k_{t2}$	$k_{t1}k_{c2}k_{c2}$

The transmission matrices for the fiber coil (including PZT) have reciprocal forms [4] as Eq. (6), where C1, C2, C3, and C4 are complex coefficients.

$$\mathbf{M}^{+}=\begin{bmatrix} C_1 & C_2 \\ C_3 & C_4 \end{bmatrix},\quad \mathbf{M}^{-}=\begin{bmatrix} C_1 & C_3 \\ C_2 & C_4 \end{bmatrix}. \tag{6}$$

Light intensity and PN errors of each path can be derived by Eq. (7), where $\phi=\phi_S+\Delta\phi(t)$ includes both the Sagnac phase ϕ_S and the modulation phase $\Delta\phi(t)$.

$$\begin{aligned} \mathbf{E}_{ij}^{+} &= \mathbf{w}_n^{+}\mathbf{P}_j\mathbf{M}^{+}\mathbf{P}_i\mathbf{E}_0 e^{j\phi},\quad \mathbf{E}_{ij}^{-}=\mathbf{w}_n^{-}\mathbf{P}_j\mathbf{M}^{-}\mathbf{P}_i\mathbf{E}_0 \\ \mathbf{I}_{ij}^{n} &= \left\langle \left|\mathbf{E}_{ij}^{+}+\mathbf{E}_{ij}^{-}\right|^2 \right\rangle = I_0+q_n\cos\phi+p_n\sin\phi = I_0+\sqrt{p_n^2+q_n^2}\cos\left(\phi-\phi_{err}^{n}\right) \\ \phi_{err}^{n} &= \arctan(p_n/q_n). \end{aligned} \tag{7}$$

Here, I_0 is a direct-current component unrelated to the rotation rate. The subscripts "*i*" and "*j*" stand for polarization states, and thus "*ij*" implies light waves couple from polarization *i* to *j*. Assuming the polarizers have high PER, we neglect high order polarization coupling.

The parameters p_n and q_n of each path are given in Eq. (8). Here $u_1=|C_2^*C_1|\cos\phi_{21}+|C_1^*C_3|\cos\phi_{13}$ and $u_2=|C_2^*C_1|\sin\phi_{21}+|C_1^*C_3|\sin\phi_{13}$, in which ϕ_{13} and ϕ_{21} are additional phases induced by $C_1^*C_3$ and $C_2^*C_1$ respectively.

$$\begin{aligned} p_1 &= p_1^c=-w_1\varepsilon_x u_2, & q_1 &= w_1|C_1|^2+w_1\varepsilon_x u_1 \\ p_2 &= p_2^c=-w_2\varepsilon_y u_2, & q_2 &= w_2|C_4|^2-w_2\varepsilon_y u_1 \\ p_3 &= p_3^c+p_3^s=w_2\varepsilon_y u_2-w_2\left|C_3^*C_2\right|^2\sin\phi_{32}, & q_3 &= -w_2\left|C_3^*C_2\right|^2\cos\phi_{32}-w_2\varepsilon_y u_1 \\ p_4 &= p_4^c+p_4^s=w_1\varepsilon_x u_2+w_1\left|C_3^*C_2\right|^2\sin\phi_{32}, & q_4 &= -w_1\left|C_3^*C_2\right|^2\cos\phi_{32}+w_1\varepsilon_x u_1. \end{aligned} \tag{8}$$

We classify the PN errors into two categories ϕ_n^s and ϕ_n^c, according to the number of polarizers in their respective light paths. Therefore, p_n described in Eq. (8) can be decomposed into p_n^c and p_n^s according to whether the component contains ε. Hence, $\phi_n^s=\arctan(p_n^s/q_n)$ and $\phi_n^c=\arctan(p_n^c/q_n)$. It is obvious that ϕ_3^s and ϕ_4^s have opposite phases, given by

$$\phi_3^s=\arctan\left(\frac{\left|C_3^*C_2\right|^2\sin\phi_{32}}{\left|C_3^*C_2\right|^2\cos\phi_{32}+\varepsilon_y u_1}\right),\quad \phi_4^s=-\arctan\left(\frac{\left|C_3^*C_2\right|^2\sin\phi_{32}}{\left|C_3^*C_2\right|^2\cos\phi_{32}-\varepsilon_x u_1}\right). \tag{9}$$

Besides, the PN errors ϕ_1^c and ϕ_2^c in reciprocal paths have opposite signs to the PN errors ϕ_3^c and ϕ_4^c in nonreciprocal paths, given by

$$\begin{aligned} \phi_1^c &= \arctan\left(\frac{-\varepsilon_x u_2}{|C_1|^2+\varepsilon_x u_1}\right),\quad \phi_2^c=\arctan\left(\frac{-\varepsilon_y u_2}{|C_4|^2-\varepsilon_y u_1}\right) \\ \phi_3^c &= \arctan\left(\frac{\varepsilon_y u_2}{-\left|C_3^*C_2\right|^2\cos\phi_{32}-\varepsilon_y u_1}\right),\quad \phi_4^c=\arctan\left(\frac{\varepsilon_x u_2}{-\left|C_3^*C_2\right|^2\cos\phi_{32}+\varepsilon_x u_1}\right). \end{aligned} \tag{10}$$

The optical delay line ensures the two polarizations are incoherent, and hence, PN errors of two PDs can be derived as

$$\begin{aligned} \phi_{err}^{pd1} &= \arctan\frac{p_1+p_3}{q_1+q_3}=\arctan\frac{-w_2\left|C_3^*C_2\right|^2\sin\phi_{32}+(w_2\varepsilon_y-w_1\varepsilon_x)u_2}{w_1|C_1|^2-w_2\left|C_3^*C_2\right|^2\cos\phi_{32}+(w_1\varepsilon_x-w_2\varepsilon_y)u_1} \\ \phi_{err}^{pd2} &= \arctan\frac{p_2+p_4}{q_2+q_4}=\arctan\frac{w_1\left|C_3^*C_2\right|^2\sin\phi_{32}-(w_2\varepsilon_y-w_1\varepsilon_x)u_2}{w_2|C_4|^2-w_1\left|C_3^*C_2\right|^2\cos\phi_{32}+(w_1\varepsilon_x-w_2\varepsilon_y)u_1}. \end{aligned} \tag{11}$$

When we add results of two PDs directly, light intensity and PN errors of multiple compensation IFOG are calculated as

$$I_{sum}=\sum_{n=1}^{4} I_{ij}^{n}=I_0+\left(\sum_{n=1}^{4} q_n\right)\cos\phi+\left(\sum_{n=1}^{4} p_n\right)\sin\phi=I_0+\sqrt{\left(\sum_{n=1}^{4} p_n\right)^2+\left(\sum_{n=1}^{4} q_n\right)^2}\cos\left(\phi-\phi_{err}^{sum}\right)$$

$$\phi_{err}^{sum}=\arctan\frac{\sum_{n=1}^{4} p_n}{\sum_{n=1}^{4} q_n}=\arctan\frac{(w_1-w_2)\left|C_3^* C_2\right|^2\sin\phi_{32}}{w_1|C_1|^2+w_2|C_4|^2-(w_1+w_2)\left|C_3^* C_2\right|^2\cos\phi_{32}+2(w_1\varepsilon_x-w_2\varepsilon_y)u_1}. \quad (12)$$

References

[1] E. J. Post, "Sagnac effect," *Rev. Mod. Phys.*, vol. 39, no. 2, pp. 475–493, Apr. 1967.
[2] H. C. Lefèvre, *The Fiber-Optic Gyroscope*. Norwood, MA, USA: Artech House, 1993.
[3] V. Vali and R. W. Shorthill, " Fiber ring interferometer," *Appl. Opt.*, vol. 15, no. 5, pp. 1099–1100, May 1976.
[4] I. A. Andronova and G. B. Malykin, "Physical problems of fiber gyroscopy based on the Sagnac effect," *Phys. Usp.*, vol. 45, no. 9, pp. 793–817, Aug. 2002.
[5] R. Ulrich, "Fiber-optic rotation sensing with low drift," *Opt. Lett.*, vol. 5, no. 5, pp. 173–175, May 1980.
[6] R. Ulrich and M. Johnson, "Fiber-ring interferometer—Polarization analysis," *Opt. Lett.*, vol. 4, no. 5, pp. 152–154, May 1979.
[7] D. Kim and J. Kang, "Sagnac loop interferometer based on polarization maintaining photonic crystal fiber with reduced temperature sensitivity," *Opt. Exp.*, vol. 12, no. 19, pp. 4490–4495, Sep. 2004.
[8] E. Jones and J. W. Parker, "Bias reduction by polarisation dispersion in the fibre-optic gyroscope," *Electron. Lett.*, vol. 22, no. 1, pp. 54–56, Jan. 1986.
[9] B. Szafraniec and J. Blake, "Polarization modulation errors in all-fiber depolarized gyroscopes," *J. Lightw. Technol.*, vol. 12, no. 9, pp. 1679–1684, Sep. 1994.
[10] B. Szafraniec and G. A. Sanders, "Theory of polarization evolution in interferometric fiber-optic depolarized gyros," *J. Lightw. Technol.*, vol. 17, no. 4, pp. 579–590, Apr. 1999.
[11] Y. Yang, Z. Wang, and Z. Li, "Optically compensated dual-polarization interferometric fiber-optic gyroscope," *Opt. Lett.*, vol. 37, no. 14, pp. 2841–2843, Jul. 2012.
[12] Z. Wang *et al.*, "All-depolarized interferometric fiber-optic gyroscope based on optical compensation," *IEEE Photon. J.*, vol. 6, no. 1, pp. 7100208, Feb. 2014.
[13] Z. Wang *et al.*, "Optically compensated polarization reciprocity in interferometric fiber-optic gyroscopes," *Opt. Exp.*, vol. 22, no. 5, pp. 4910–4919, Feb. 2014.
[14] Z. Wang *et al.*, "Dual-polarization interferometric fiber-optic gyroscope with an ultra-simple configuration," *Opt. Lett.*, vol. 39, no. 8, pp. 2463–2466, Apr. 2014.
[15] S. L. A. Carrara, B. Y. Kim, and H. J. Shaw, "Bias drift reduction in polarization-maintaining fiber gyroscope," *Opt. Lett.*, vol. 12, no. 3, pp. 214–216, Mar. 1987.